



*QUICS: Quantifying Uncertainty in Integrated
Catchment Studies*

*D2.2 Report on software tools for investigating
the influence of hydraulic structures and their
uncertainty in sewer network modelling*

Lead Partner: UC

Revision: 30th May 2018

Report Details

Title: Software tools for investigating the influence of hydraulic structures and their uncertainty in sewer network modelling

Deliverable Number: 2.2

Authors: Md Nazmul Azim Beg (NB), Rita F. Carvalho (RFC), Jorge Leandro (JL), Alma Schellart (AS)

Dissemination Level: Public

Document History

Version	Date	Status	Submitted by	Checked by	Comment
	12.06.2017		Rita Carvalho	Nazmul Beg and Jorge Leandro	RFC proposed outline
V 1.0	10.07.2017		Nazmul Beg	Rita Carvalho	NB added Chapter 3, 5, 6 and 7 and part of Chapter 2
V 1.1	11.07.2017		Rita Carvalho	Jorge Leandro	RFC added Chapter 1 and 2, revised Chapter 3, 5, 6 and 7
V 1.2	11.07.2017		Jorge Leandro	Rita Carvalho	JL proposed Chapter 4
V 1.3	12.07.2017		Nazmul Beg	Rita Carvalho and Jorge Leandro	NB modified Chapter 4
V 1.4	21.07.2017	First Draft	Rita Carvalho	Jorge Leandro	RFC revised and compiled all chapters, JL advised to change Figure 1
V 1.5	21.07.2017		Nazmul Beg	Lutz Breuer and Alma Schellart	NB corrected Figure 1 Lutz Breuer suggested adaptations to the report structure and witting
V1.6	15.03.2018		Alma Schellart	Nazmul Beg and Rita Carvalho	AS suggested text edits and suggested adaptations to the report structure, including moving some background chapters to appendices.
V 2.0	04.05.2018	Draft	Nazmul Beg	Rita Carvalho and Jorge Leandro	NB and RFC discussed suggestions and changed according to the previous check, NB shortened the report, added appendix, added some more results in new chapter 2
V 2.1	07.05.2018		Rita Carvalho	Simon Tait	RC organized parts and did text alterations
V2.2	27.05.18	Final	Simon Tait	Rita Carvalho	Final check

ACRONYMS AND ABBREVIATIONS

1D	One Dimensional
2D	Two Dimensional
3D	Three Dimensional
ADV	Acoustic Doppler Velocimetry
ASM	Algebraic Stress Models
CFD	Computational Fluid Dynamics
CSCM	Coherent Structure Capturing Model
DNS	Direct Numerical Simulation
FDM	Finite Differences Methods
FVM	Finite Volumes Method
GUI	Graphical User Interface
LES	Large Eddy Simulation
OpenFOAM®	Registered trademark a CFD tool box naming: Open source Field Operation And Manipulation
PDF	Probability Density Function
PIV	Particle Image Velocimetry
RANS	Reynolds Averaged Navier–Stokes
RSM	Reynolds Stress Models
SGS	Sub-Grid Scale
STL	Stereo Lithography file
SWE	Shallow Water Equations
SVE	Saint-Venant Equations
TUM	Technical University of Munich
UC	University of Coimbra
VOF	Volume Of Fluid

Acknowledgements



This project has received funding from the European Union's Seventh Framework Programme for research, technological development and demonstration under grant agreement no 607000.

EXECUTIVE SUMMARY

This report contains an overview of the use of the OpenFOAM® Toolbox which has been used to simulate 3D flows in different hydraulic structures commonly found in urban drainage systems. The report describes the results of the different simulations of full-scale manholes and street gullies that were carried out for a range of hydraulic conditions. Experimental research was performed in laboratories at the University of Coimbra and the University of Sheffield. In the laboratories, velocity and head measurements to validate the performance of OpenFOAM in simulating the 3D flows in these structures was obtained. Data analysis was carried out of the 3D OpenFOAM simulations in order to achieve head loss and discharge coefficients, which are two fundamental characteristics to model successfully such urban drainage structures in 1D and 2D models. Uncertainty involved in calculating these values considering their detailed geometric shape and different flow conditions are also analysed. This demonstrated that small deviations in the alignment of the inflows and outflows, and small changes in a manhole geometry could produce large changes in head loss and discharge coefficients. These results suggest that such uncertainties could have a significant impact on flow simulations in 1D network models and further modelling with 1D models with a range of headloss and discharge coefficients is recommended.

CONTENTS

Acronyms and Abbreviations	3
Executive Summary	4
Contents	5
1 Introduction	7
1.1 Partners Involved in Deliverable	7
1.2 Deliverable Objectives	7
1.3 Context	7
2 Using CFD tools to estimate uncertainty caused by hydraulic structures	8
2.1 Including uncertainty due to hydraulic structures modelling	8
2.2 Choice of appropriate CFD tools	9
3 Application of CFD in assessing uncertainty in the drainage structures	11
3.1 Validation of CFD model with detailed velocity measurements in the lab	11
3.2 Application in assessing manhole head loss	12
Calculation of head loss coefficients of a standard manhole at different surcharge	12
Comparison of manhole head loss coefficient for different types of manholes	13
Head loss coefficient of manhole due to different inlet connections	15
3.3 Application in assessing gully discharge coefficient	16
Discharge coefficients of a Gully at different manhole surcharge	16
Discharge coefficient of gully due to different outlet types	17
4 Conclusion	19
References	20
APPENDICES	1
APPENDIX 1 - Mathematical Models	1
Equations of Motion	1
3D Models - CFD	1
1D, 2D and quasi-3D Equations	3
APPENDIX 2 - OpenFOAM®	5
Overview of OpenFOAM®	5
Considerations of working with OpenFOAM®	6
OpenFOAM® Mesh Generation	7
Basics of Mesh Generation	7
BlockMesh	8
	5

Salomé	8
CfMesh	8
SnappyHexMesh	9
Pre-processing: Initial and Boundary Conditions	9
SOLVER	10
InterFoam solver	10
Running InterFoam solver	12
Post-Processing	13

1 INTRODUCTION

1.1 Partners Involved in Deliverable

The University of Coimbra is the main partner involved in this deliverable, with collaboration of the University of Sheffield and the Associate Partner the Technical University of Munich (TUM).

1.2 Deliverable Objectives

The aim of this report is to provide an overview of Computational Fluid Dynamics (CFD) tools that can be used to simulate flows through hydraulic structures in urban drainage systems. In the present studies two common specific structures: manholes and gullies are studied. These simulations were validated with data from two different laboratory setups at University of Sheffield and at University of Coimbra using Particle Image Velocimetry (PIV) and Acoustic Doppler Velocimetry (ADV) coupled with pressure sensor measurements. The data is used to calculate head loss and discharge coefficients which enable the study of the effects of such structures on water quality and quantity in urban drainage system models.

1.3 Context

The detailed behaviour of the flow in individual hydraulic structures in urban drainage systems, such as gullies and manholes, has attracted increasing interest, e.g. (Beg et al., 2018a; Chang et al., 2018; Lopes et al., 2017, 2016; Martins et al., 2014; Pfister and Gissoni, 2014; Stovin et al., 2013). These hydraulic structures work as linkage elements within a large network and their individual behaviour may have a strong influence of the flow of water and pollutants in urban drainage systems.

However, modelling details of three dimensional (3D) flow in all hydraulic structures in large urban drainage network models is not computationally feasible. Therefore, the influence of 3D flow is usually translated into coefficients that are incorporated into one dimensional (1D) or two dimensional (2D) as well as 1D-2D urban drainage network models. The uncertainty related to this translation of 3D flows in urban drainage structures to single 1D coefficients, has, as far as the authors are aware not been studied before. Computational Fluid Dynamics (CFD) tools such as OpenFOAM®, ANSYS-FLUENT and FLOW3D allows fully applicable simulations on complex detailed flow. Thus modelling the flow structures under different hydraulic conditions enhances knowledge on flow behaviour, which can then be widely included in other models through the use of representative coefficients. Since a wide range of models and CFD software packages are available and a particular simulation could be highly case specific, numerical simulations still need an adequate verification and validation. Constructing physical models of specific hydraulic structures, and measuring flow details is time consuming, labour intensive and expensive. A methodology based on CFD which has been tested with a limited number of physical model tests, could be widely used to achieve reasonable results and knowledge on 3D flows through hydraulic structures. Knowledge on 3D flows through different hydraulic structures allows the derivation of coefficients that can be included in 1D or 2D models for predicting specific behaviour of urban drainage system. Researching the range of potential coefficient values found could aid in describing the uncertainty caused by simplifying 3D flow structures into 1D or 2D model simulations. In Appendix 1 a review of mathematical models and equations used in 1D, 2D and 3D computational models is presented.

2 USING CFD TOOLS TO ESTIMATE UNCERTAINTY CAUSED BY HYDRAULIC STRUCTURES

2.1 Including uncertainty due to hydraulic structures modelling

When the hydraulic structures are considered in a large scale network model used to calculate flows, they are simplified and considered as a point entity. The flow and momentum exchange in a structure is taken into account by means of empirical equations and coefficients. Several sources of uncertainty may lie in choosing particular coefficient values or a particular empirical equation at a certain flow condition to translate the hydraulic structure's behaviour to a network model. Appendix 2 presents a brief description of current software for 1D and 2D models. The uncertainty quantification in this study is focused on determining an empirical formula to translate drainage manhole and gully behaviour to the network model.

There are many ways to take uncertainty into account when modelling flows through urban drainage systems. One common method involves deriving a statistical probability density function (PDF) of a certain input or model parameter, and calculating the outcome using Monte-Carlo based approaches. Later, a PDF of the possible outcomes is derived. In this methodology, to obtain a proper PDF as output, one has to simulate the model a large number of times, in the range of a few hundreds to few thousands simulations in order to converge on a stable output pdf. For this reason, mostly stochastic or 1D models are used in these cases to simulate the numerous results as they are less computationally expensive.

However, hydraulic modelling of a drainage structure using stochastic modelling is impractical as it involves complex flow phenomena and possibly multi phased flow. Traditional stochastic models or 1D models are not suitable to model adequately this complex flow. For this reason, detailed physically based models are necessary to simulate the flow. Physics based models consist of a set of mathematical equations and will always return the same output for a particular set of inputs, without considering uncertainty or randomness (Korving, 2004). These models are computationally expensive involving many model inputs and parameters and very high computational time requirement in running them.

It is therefore not realistic to use a CFD model to simulate many simulations that can construct a PDF output to assess uncertainty using traditional Monte-Carlo methods. Instead, specific sets of simulation will be tested with a view of finding the maximum and minimum possible changes in the model results due to different boundary conditions and then obtain a simple relationship to describe the uncertainty associated with the 3D hydraulic processes. When constructing a hydraulic structure in the field, a construction error may result in a geometrical error that could be responsible for changing the hydraulic performance compared to the performance anticipated in the planned design. Considering these issues, our research focuses on finding uncertainties due to:

- Head loss coefficients of manholes at
 - different surcharge conditions
 - different manhole types
 - different inlet orientations
- Discharge coefficient of the inlet gully for
 - different gully pipe and surcharge conditions
 - different gully outlet types

In applying hydraulic model for manholes and gullies, the aim is to find the specific coefficients and their ranges of uncertainty that is important to be included in a 1D network model. Head loss coefficients for

manholes and discharge coefficients for gullies are two of such parameters that are frequently used to represent these structures behaviour in a simplified 1D model. In this research, we focused on the uncertainty in calculating them.

As a CFD model uses many parameters and offers many options to choose the parametric values, work will also be done to select the right parameter with the right parametric values by comparing simulation data with experimental laboratory results. This report focused on choosing the appropriate turbulence model for a manhole, by comparing the model velocity and pressure data with experimental PIV data and data from pressure sensors. After considering different cases in CFD and laboratory results, manhole head loss coefficients and gully discharge coefficients will be proposed to be tested in 1D and 2D network models by future researchers.

2.2 Choice of appropriate CFD tools

CFD software solves the governing equations of fluid motion, consisting of equations describing mass, momentum and energy conservation, in order to obtain transient, three-dimensional solutions. Averaging or filtering the Navier-Stokes equations (Eq. 1, 2 and 3) is current practice in hydraulic engineering applications.

$$\frac{\partial \rho}{\partial t} + \nabla \cdot (\rho u) = 0 \quad (1)$$

$$\frac{\partial \rho u}{\partial t} + \nabla \cdot (\rho u u) = \rho g + \nabla \cdot \sigma \quad (2)$$

$$\frac{\partial \rho e}{\partial t} + \nabla \cdot (\rho e u) = \rho g u + \nabla \cdot (\sigma u) - \nabla \cdot q + \rho Q \quad (3)$$

To model flow in a hydraulic structure in an unpressurised system a free surface simulation needs to be included in the model. To model the free surface flow accurately, the volume of fluid (VOF) method (Hirt and Nichols, 1981) is considered one of the best options (Carvalho et al., 2008). Several CFD tools are available that have the VOF method included. The following gives a basic overview of the available software tools that incorporate free surface simulation.

FLOW-3D

FLOW-3D® is a general purpose CFD commercial software tool with a Graphical User Interface (GUI) that solves the governing equations of fluid motion to obtain transient, three-dimensional solutions. FLOW-3D® has been extensively used in hydraulic engineering applications. FLOW-3D uses Finite Volume Method (FVM)/Finite Differences Methods (FDM) to solve the equations of fluid motion in a Cartesian staggered grid. The Fractional Area/Volume Obstacle Representation (Hirt and Sicilian, 1985), named FAVOR™ method is one of the major features of FLOW-3D. In this tool, obstacles are modelled as zero-volume porosity regions, and the six components of wall shear stress are included implicitly in the equations to avoid numerical instabilities.

FLUENT/ANSYS

ANSYS Fluent is one of the most popular CFD software tools. Similar to FLOW-3D, it is also a commercial software tool and comes with a GUI. The software package includes well-validated physical modelling capabilities that are able to deliver fast, accurate results for a very wide range of multi-physics applications. Along with ANSYS Fluent another primary ANSYS product is ANSYS CFX. With the combined capabilities of these products, one can simulate a wide range of phenomena: aerodynamics, combustion, hydrodynamics, mixtures of liquids/solids/gas, particle dispersions, reacting flows, heat transfer, and much more. Steady-state and transient flow phenomena are easily and quickly solved. For fluid interaction, ANSYS Fluent offers

finite volume based 2D and 3D simulation results at both staggered and non-staggered grids. The software package has different solvers to give solutions of multi-phase physical and chemical analysis (ANSYS Inc, 2013).

OpenFOAM®

OpenFOAM® meaning "Open source Field Operation And Manipulation" is a freely available open source platform containing several C++ libraries and applications which can numerically solve continuum mechanics problems (Weller et al., 1998). Its implementation is based on a tensorial approach using object-oriented programming techniques and the FVM. The toolbox enable the development of customised numerical solvers, and contains pre and post-processing utilities.

Unlike the first two mentioned software packages OpenFOAM is freely available and probably contains the biggest library of solvers to choose from. On top of that, OpenFOAM has its source code freely available. This made it popular with researchers as they can adapt the codes according to their needs. Considering these issues, OpenFOAM is chosen for our research work to consider uncertainty in drainage structures.

Out of several solvers OpenFOAM offers, the interFoam solver is chosen for our research work. This solver includes a VOF method to model free surfaces which is ideal for flow in urban drainage systems. Several turbulence models can be applied within this solver. Moreover, the code of interFoam solver can be optimized with added equations to calculate solute and/or suspended materials if needed.

A brief description of the OpenFOAM toolbox is presented in the Appendix 2. This appendix provides readers with the essential information on how to construct models in OpenFOAM and to start to use them.

3 APPLICATION OF CFD IN ASSESSING UNCERTAINTY IN THE DRAINAGE STRUCTURES

3.1 Validation of CFD model with detailed velocity measurements in the lab

Use of validated CFD modelling methodologies to analyse flow behaviour is in widespread engineering practice. In this research study, flow behaviour in a scaled manhole was analysed using stereo PIV. This method, illustrated in Figure 1a, uses two cameras to record particle images in a 2D plane to calculate three components of velocity vectors in the flow. The recorded data in three planes (Figure 1b) was compared with commonly used four different Reynolds Averaged Navier–Stokes (RANS) models to find the best modelling procedure to simulate manhole hydraulics. The comparative results at the central plan are shown in Figure 1b. Comparison of flow velocity and water level between CFD and experimental data showed that the re-normalization group (RNG) k-ε model gives the best approximation for manhole velocity and pressure (Beg et al., 2018b).

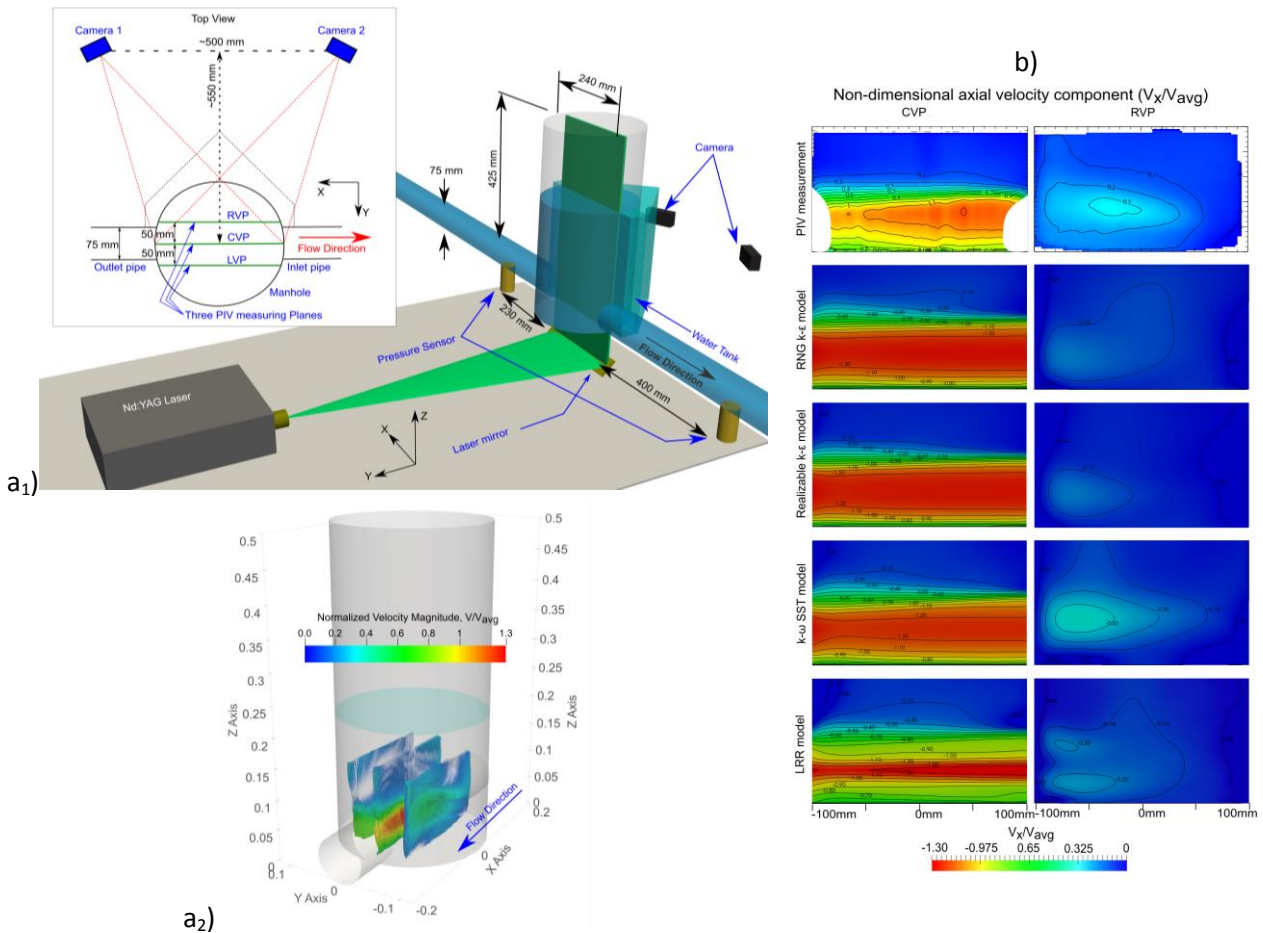


Figure 1: a₁) Lab setup for utilizing PIV in a scaled manhole, a₂) Plans definition and b) Measured velocity data in the manhole showing anti clockwise from left; comparison between measured velocity and CFD results (Beg et al., 2018b)

In the next step of the work, the RNG k-ε model was utilized to model flow behaviour of a prototype manhole. Experimental measurements of pressure and water level were obtained at the bottom of the manhole as well as at the inlet and outlet pipes. Experimental measurement was also collected in a prototype gully using an ADV (Figure 2). All the measurements were compared with CFD model results (Beg et al., 2018a).

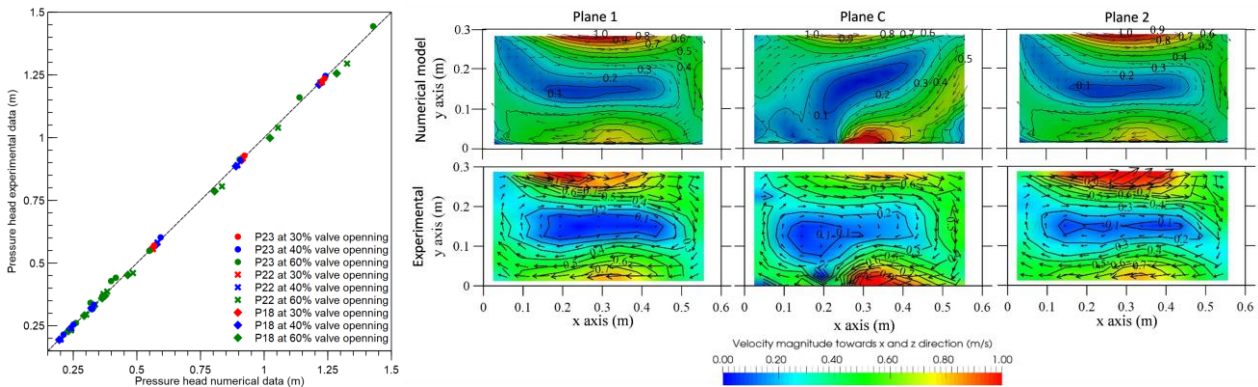


Figure 2: Left panel: comparison of pressure and water level at a prototype manhole, Right panel: comparison of flow in a prototype gully (Beg et al., 2018a)

3.2 Application in assessing manhole head loss

Calculation of head loss coefficients of a standard manhole at different surcharge

A validated CFD model has been used to calculate head loss in a prototype manhole. The solver interFoam has been utilised to study the flow phenomena in different urban hydraulic structures.

OpenFOAM® with the solver interFoam was employed to examine the head loss coefficient of a 1:1 scale standard manhole. Figure 3 shows the computational domain of the CFD model, which replicates a physical model setup installed at the University of Coimbra. The model consists of a manhole of 1 m diameter (\varnothing_m), connected with a 300 mm coaxial inlet-outlet pipe as well as 0.48 m gully and surface drain.

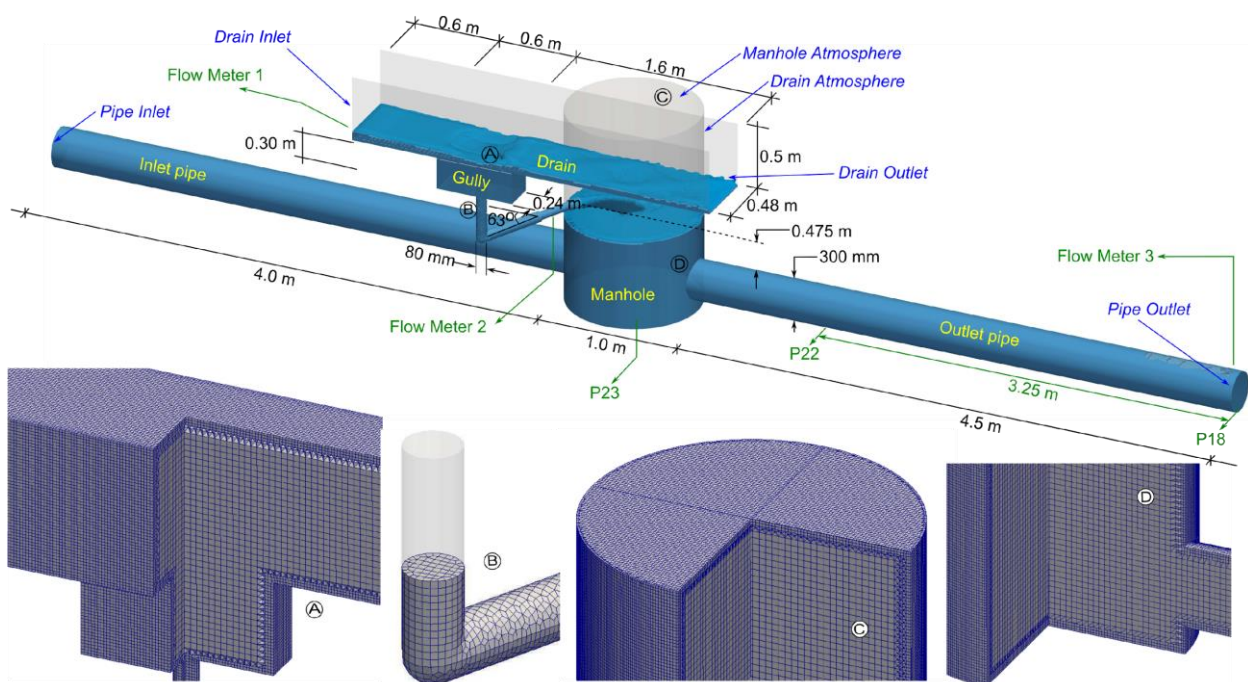


Figure 3: Computational domain for OpenFOAM model of gully and manhole (Beg et al., 2018a)

When the flow of an inlet pipe enters a manhole, the flow expands and later contracts while exiting through an outlet pipe. Due to this expansion and contraction, the flow loses a portion of its energy. Quantification of this energy loss is considered important for urban drainage modelling. The manhole head loss coefficients were calculated for different inflows and different surcharge conditions. The head loss coefficient (K) was calculated as a ratio between the water column head loss (ΔH) and velocity head of the flow; using the following equation:

$$K = \frac{\Delta H}{v^2/2g} \quad (4)$$

Where, v is the average velocity at the outlet.

The value was plotted (Figure 4 Right panel) against different surcharge ratios, defined as:

$$\text{surcharge ratio} = \frac{\text{Depth of water at the inlet pipe soffit level } (s)}{\text{diameter of the inlet pipe } (\phi_p)} \quad (5)$$

Figure 4 shows the calculation of surcharge at a manhole and variation of manhole head loss coefficients at different surcharge ratios.

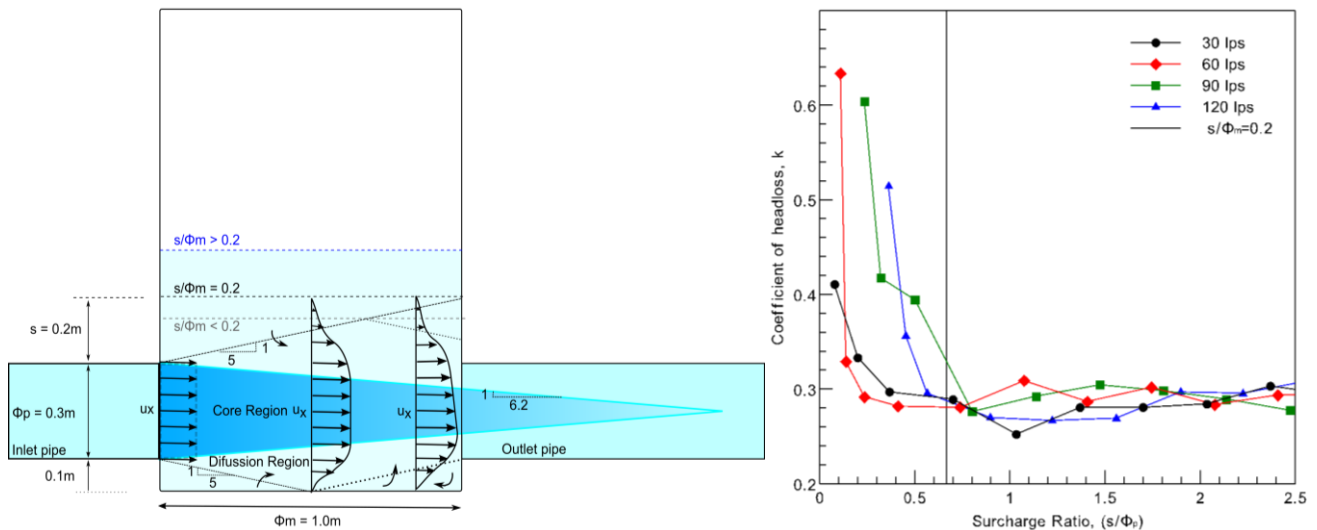


Figure 4: A manhole at surcharge condition (left) and Head loss coefficient of a manhole at for different discharge and surcharge conditions

The results showed that at high manhole surcharge condition, when the surcharge is more than 20% of the manhole diameter, the head loss coefficient is around 0.3 for all types of inflows. But at very low surcharge, the head loss increases significantly at lower surcharge ratios. Different inflows show different head loss coefficients at low surcharge condition, ranging from 0.3 to 0.65.

Comparison of manhole head loss coefficient for different types of manholes

The value of the above mentioned manhole head loss coefficient is significantly affected by the geometrical shape of a manhole. Different cities use different types of manhole due to diverse design standards. The effect of variation on manhole head loss coefficients was also examined and compared for three types of commonly found manholes, using the OpenFOAM CFD model (Beg et al., 2017). The first manhole (Type A) is

the same as explained in the previous section and presented at Figure 3. The other two types (Type B and Type C) have some structural differences (Figure 5). Type B does not have a depression and its bottom level is merged with the inlet pipe invert. Type C manhole has a more hydraulically shaped bottom. The inflow into the connection pipes is further restricted and has a more complex interior geometric shape with a guided flow channel where the channel is a U-type invert. These manholes (Type B and C) have the same dimensions (height and bottom diameter) as the previous one (Type A), except the manhole floor is different.

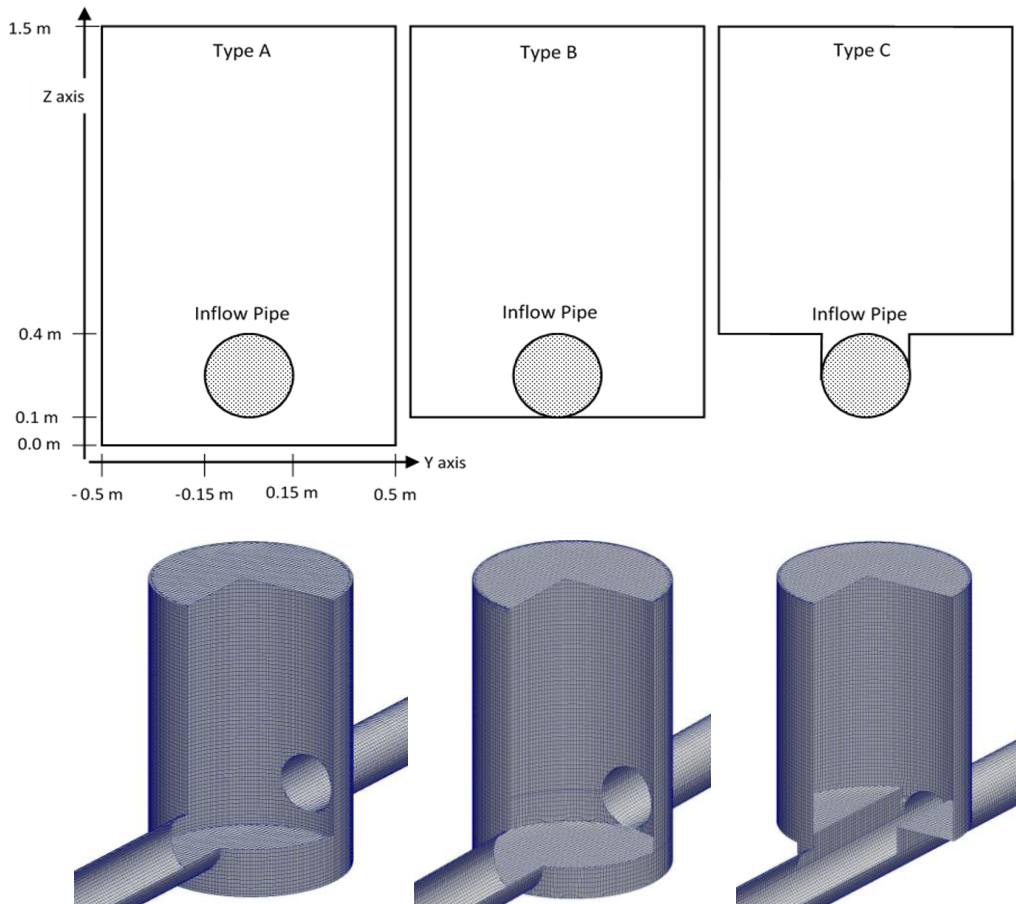


Figure 5: Schematic views of the sides of the three manholes showing sizes and positions of different components (top panel) and the computational meshes (bottom panel) (Beg et al., 2017)

The value of the head loss coefficient of these three manhole types was calculated from OpenFOAM simulations for different inlet discharge and surcharge conditions. The results are shown in Figure 6.

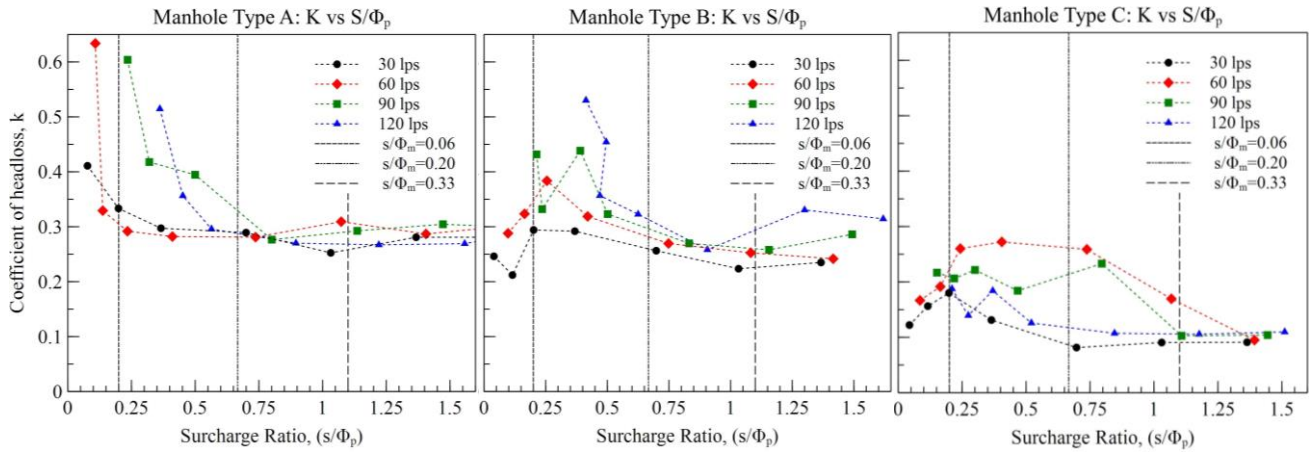


Figure 6: Head loss coefficient of three different manhole types; from left to right: Type A, B and C (Beg et al., 2017)

Analysis showed that Type C has the lowest head loss coefficient, Type C is therefore the most hydraulically efficient out of the three examined manholes. All the three types of manhole showed lower head loss coefficient at low surcharge conditions. Type A and B manholes showed high head loss coefficient at a surcharge lower than 20% of their diameter. Whereas Type C manhole showed a high head loss coefficient at surcharge lower than 33% of its diameter.

Head loss coefficient of manhole due to different inlet connections

Uncertainty may arise from different inlet and outlet orientations of the manhole. To investigate this case, four additional CFD models were constructed using Manhole Type A. However, these were not inline manholes. Each inlet and outlet pipes for these cases were horizontal but they made an angle of 2°, 5°, 10° and 15° respectively between them. These new four manholes were simulated for different inflow and surcharge conditions and corresponding coefficient of head losses were calculated (Figure 7).

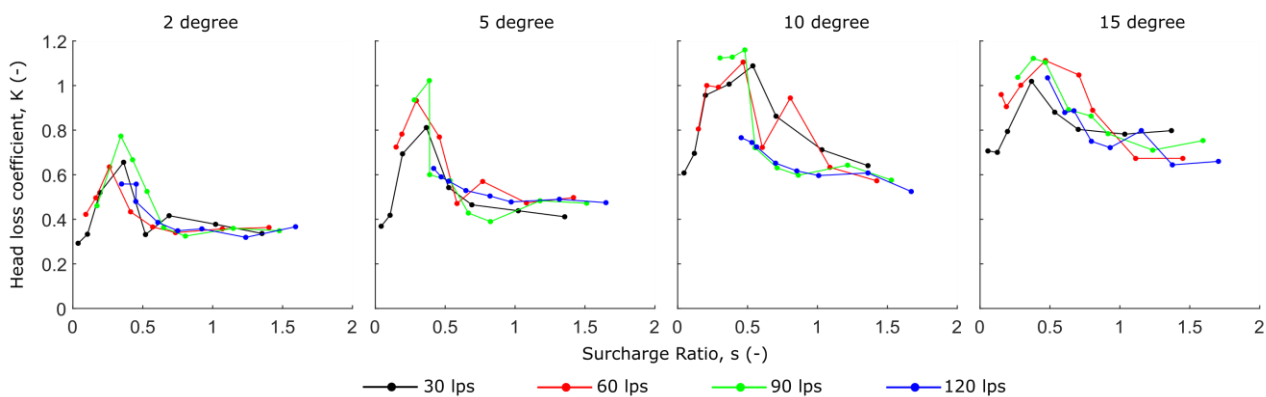


Figure 7: Head loss coefficient due to change in horizontal orientation angle between inlet and outlet

Analysis showed that with the change in horizontal orientation angles, the value of the head loss coefficient increases. In inline manholes as the fast flowing jet flow passes directly through to the outlet pipe. Whenever, the inlet and outlet pipes are not oriented in one direction, the incoming jet hits the opposite wall of the manhole and reduces the jet velocity. As a result, the manhole head loss increases.

3.3 Application in assessing gully discharge coefficient

Discharge coefficients of a Gully at different manhole surcharge

During a rainfall event, a roadside gully collects the runoff from the road and discharges this to a nearby manhole. In the case of heavy rainfall conditions, the manhole may become surcharged and sometimes the surcharge height may control the drainage flow from the street gully.

A study was carried out to examine the gully discharge at different surcharge conditions of a manhole using OpenFOAM® utilizing the interFoam solver. The same physical model setup and computational domain shown in Figure 3, was used for this study. Inflow was applied at the drain inlet with different surcharge levels at the manhole. The corresponding discharge through the gully outlet was recorded from the CFD models. For a certain hydraulic conditions, time averaged point velocities in the gully were recorded at a number of locations and the data spatially interpolated. The CFD velocity was validated using the velocity data as shown in Figure 2.

CFD results showed three different surcharge zones in the manhole (Figure 8) at which the gully outlet flow acts differently. At Zone 1, the gully discharge is a free outlet; at Zone 2, the gully discharge acts like a submerged jet and at Zone 3, the manhole surcharge creates reverse flow at the gully.

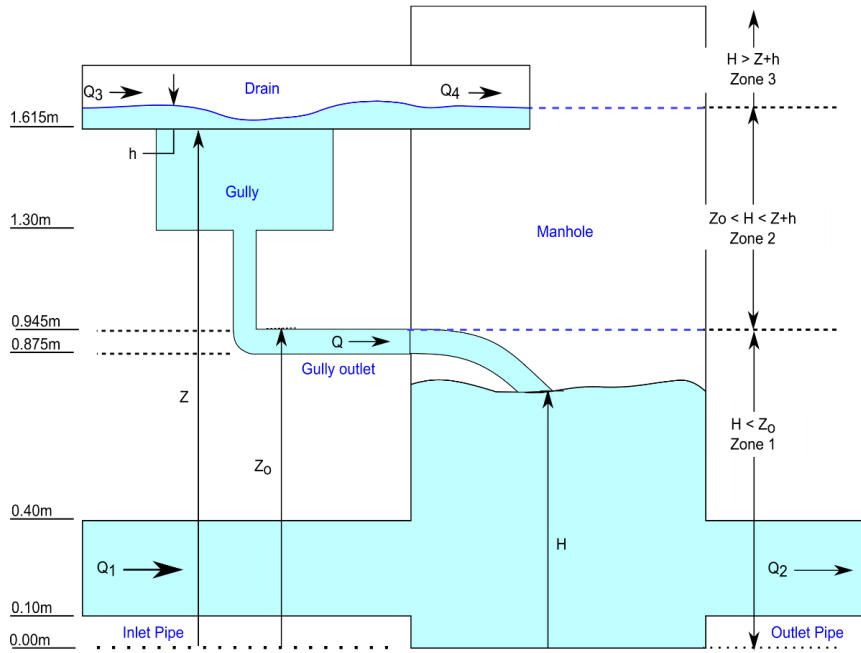


Figure 8: Different surcharge zone of the manhole

The flow through the gully was found to follow the orifice rule, using the following equation:

$$Q = C_d A \sqrt{2gH} \quad (6)$$

Where C_d is the discharge coefficient being investigated, A is the cross sectional area of the gully outlet, H is the head difference and g is the gravitational acceleration.

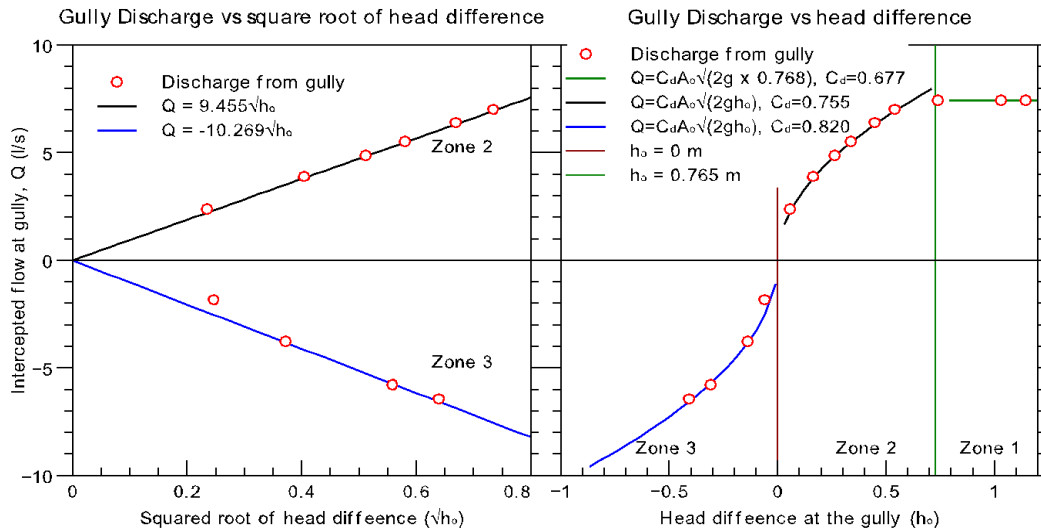


Figure 9: Calculation of different discharge coefficients of the gully at different manhole surcharge

It has been seen that the CFD predicted value of the coefficient of discharge at the gully outlet was different for the three surcharge zones. The discharge vs head difference was plotted (Figure 9) for all the scenarios tested. The discharge coefficients were calculated from the drawn best-fitted curves and found as shown in Table 1.

Table 1: Discharge coefficient of the gully outlet for different surcharge conditions

Zone	C_d	Remarks
Zone 1	0.677	Free outfall to the atmosphere, like a plunging jet to the manhole
Zone 2	0.755	Submerged jet condition
Zone 3	0.820	Reverse flow from manhole to the gully

Discharge coefficient of gully due to different outlet types

The discharge coefficients of a gully showed different values due to the gully outlet pipes types. Two different characteristics were investigated using validated CFD models: the influence of gully outlet pipe diameter and the influence of orientation angle of gully outlet.

In the first models, four different CFD gully models were constructed having outlet diameters of 80 mm, 100 mm, 150 mm and 200 mm. Each model was employed for different surcharge and inflow conditions. All the tested conditions fall in the submerged jet condition region as described in the previous section (Zone 2).

The results showed that the discharge coefficients are different at different head differences at the gully outlet. The coefficient increases with an increase in gully head difference in the submerged condition. But it tends to become constant at high head differences. With the increase in outlet pipe diameter, the coefficient increases even more. At the test case of 200 mm pipe, it was found that the coefficient of discharge drops at a high head difference. It was due to the fact that at high outlet condition, the pipe outlet collects a lot of entrapped air with the flow. This effectively reduces the available cross section area of the flow and reduces gully discharge coefficient.

For the second test set, four different gully models were constructed using validated CFD model, each having outlet pipe of 150 mm but different outlet orientation angle with the horizontal plane: 0 degree (horizontal

outlet), 15 degree, 30 degree and 45 degree. A number of tests were checked for different head difference conditions, however all the tested cases fell within Zone 2 scenario as described above.

In these test result set, it was found that like previous tests, the coefficient of discharge increases with higher heads. However, at this condition at high head difference, the coefficients showed an increasing trend. With the increase in slope angles, the discharge coefficients showed an increasing trend.

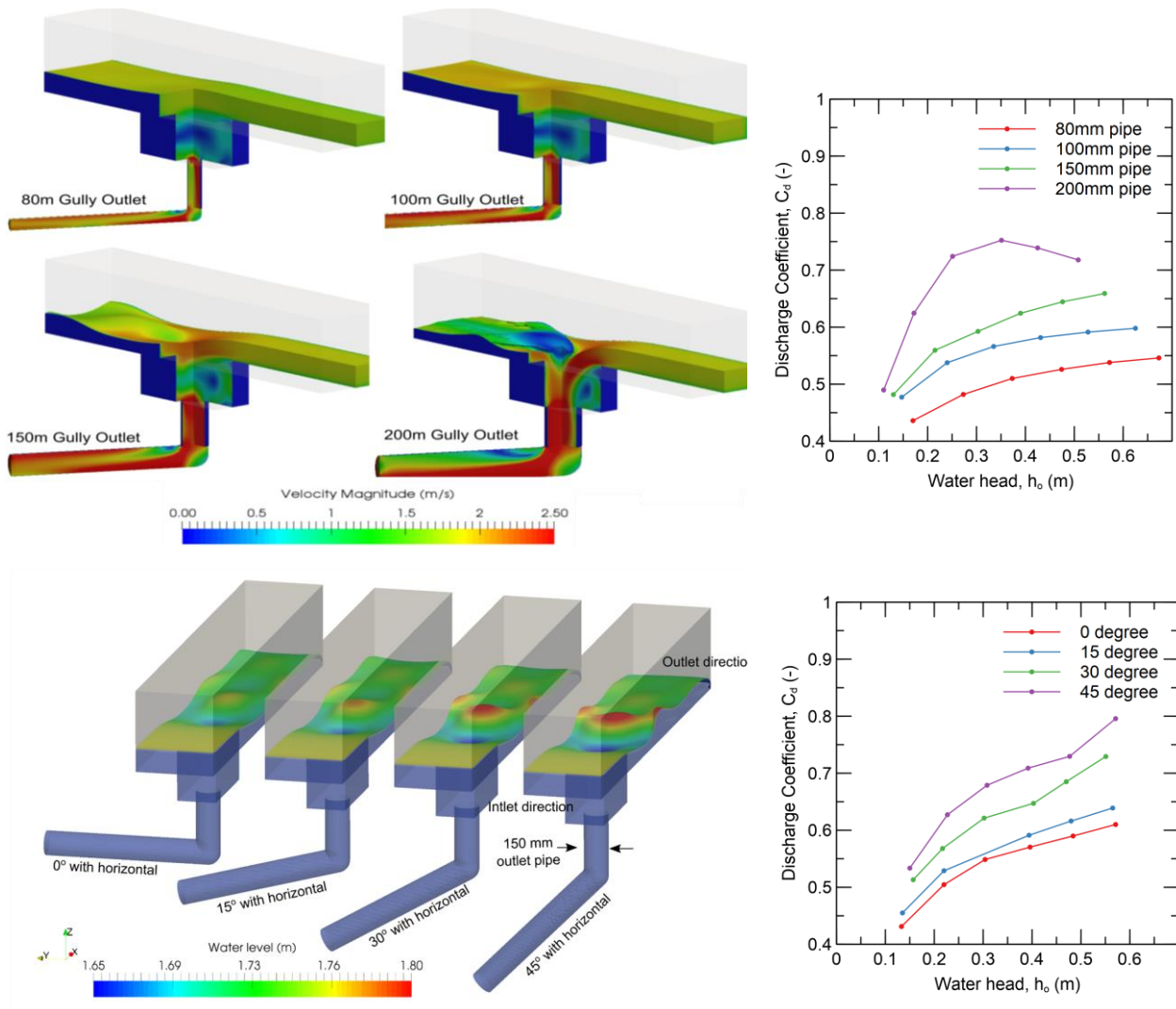


Figure 10: Different discharge coefficient due to different outlet pipe diameter (upper panel) and angles of the outlet (bottom panel)

4 CONCLUSION

The aim of this report is to present tools and software that can model flows through the hydraulic structures in urban drainage systems using CFD as well as presenting studies estimating the values of head loss and discharge coefficients that can be used in 1D-2D models so as to assess the influence of such structures on the simulation of flows in 1D hydrodynamic network models.

The most common hydraulic structures in urban drainage systems, such as gullies and manholes were simulated and validated by measurements in physical models using in University of Coimbra and Sheffield.

CFD Investigations were conducted to investigate the impact of different hydraulic structure characteristics such as geometries and inlet-outlet conditions of the predicted values of head loss and discharge coefficients. These simulations were used to quantify the ranges of uncertainty due to these changes for various hydraulic conditions. These simulations indicated that for a 5-15° directional offset of the inlet and outlet pipe a 40% difference in the head loss co-efficient was predicted, and for the different geometrical types of manhole examined very significant head loss differences were observed even if the manhole geometry differences seemed minor. This knowledge can be incorporated in widely used 1D/2D models to evaluate the impact of geometric uncertainty on flows in urban drainage systems.

Modelling of other structures in different urban systems, can follow the methodology presented herein using CFD tools combined with the use of other physical models for validation. Simulations using different details of geometry and flow conditions could be performed to achieve estimates of ranges of uncertainty that in turn can be used to integrate uncertainty into 1D sewer network hydrodynamic models.

Given these conclusions it is suggested that the following topics should be studied using the tools described in this deliverable. The calculated head loss and discharge coefficients could be applied in 1D or 2D dual drainage network models to examine the influence of hydraulics structures on the assessment of flood risk. Pollutant transport process can also be investigated in CFD as multiphase flow and discrete particles in hydraulic structures simulations can be used as well in 1D or 2D dual drainage models in order to examine the influence of geometric uncertainties in manhole on predicted water quality in urban drainage systems.

REFERENCES

- ANSYS Inc, 2013. ANSYS Fluent Theory Guide, ANSYS Inc., USA. Canonsburg, PA, USA.
- Batchelor, G.K., 1967. An Introduction to Fluid Dynamics. Cambridge University Press.
- Beg, M.N.A., Carvalho, R.F., Leandro, J., 2018a. Effect of surcharge on gully-manhole flow. *J. Hydro-environment Res.* 19, 224–236. <https://doi.org/10.1016/j.jher.2017.08.003>
- Beg, M.N.A., Carvalho, R.F., Tait, S., Brevis, W., Rubinato, M., Schellart, A., Leandro, J., 2018b. A comparative study of manhole hydraulics using stereoscopic PIV and different RANS models. *Water Sci. Technol.* 2017, 87–98. <https://doi.org/10.2166/wst.2018.089>
- Beg, M.N.A., Carvalho, R.F., Leandro, J., 2017. Comparison of flow hydraulics in different manhole types, in: Ghani, A.A. (Ed.), *Managing Water for Sustainable Development: Learning from the Past for the Future: Proceedings of the 37th IAHR World Congress*. IAHR & USAINS HOLDING SDN BHD, Kuala Lumpur, Malaysia, pp. 4212–4221.
- Berberovic, E., Van Hinsberg, N.P., Jakirlic, S., Roisman, I. V., Tropea, C., 2009. Drop impact onto a liquid layer of finite thickness: Dynamics of the cavity evolution. *Phys. Rev. E - Stat. Nonlinear, Soft Matter Phys.* 79. <https://doi.org/10.1103/PhysRevE.79.036306>
- Brackbill, J.U., Kothe, D.B., Zemach, C., 1992. Brackbill A continuum method for modeling surface tension 1992.pdf. *J. Comput. Phys.* 100, 335–354. [https://doi.org/10.1016/0021-9991\(92\)90240-Y](https://doi.org/10.1016/0021-9991(92)90240-Y)
- Carvalho, R.F., 2002. *Acções hidrodinâmicas em estruturas hidráulicas : modelação computacional do ressalto hidráulico (in Portuguese)*. University of Coimbra.
- Carvalho, R.F., Lemos, C.M., Ramos, C.M., 2008. Numerical computation of the flow in hydraulic jump stilling basins. *J. Hydraul. Res.* 46, 739–752. <https://doi.org/10.3826/jhr.2008.2726>
- Chang, T.J., Wang, C.H., Chen, A.S., Djordjević, S., 2018. The effect of inclusion of inlets in dual drainage modelling. *J. Hydrol.* 559, 541–555. <https://doi.org/10.1016/j.jhydrol.2018.01.066>
- Djordjević, S., Prodanović, D., Maksimović, Č., Ivetić, M., Savić, D., Maksimović, C., Ivetić, M., Savić, D., 2005. SIPSON - Simulation of interaction between pipe flow and surface overland flow in networks. *Wat. Sci. Tech.* 52, 275–283. <https://doi.org/http://wst.iwaponline.com/content/52/5/275>
- Germano, M., 1992. Turbulence: the filtering approach. *J. Fluid Mech.* 238, 325–336.
- Hirt, C.W., Nichols, B.D., 1981. Volume of fluid (VOF) method for the dynamics of free boundaries. *J. Comput. Phys.* 39, 201–225. [https://doi.org/10.1016/0021-9991\(81\)90145-5](https://doi.org/10.1016/0021-9991(81)90145-5)
- Hirt, C.W., Sicilian, J.M., 1985. A porosity technique for the definition of obstacles in rectangular cell meshes, in: *4th International Conference on Numerical Ship Hydrodynamics*. Washington, DC, p. 19.
- Jasak, H., 1996. *Error Analysis and Estimation for the Finite Volume Method with Applications to Fluid Flows*. Imp. Coll. Sci. Technol. Med. University of London, London.
- Juretić, F., 2015. *cfMesh User Guide (v1.1)*. Zagreb, Croatia.
- Kolmogorov, A.N., 1941. The Local Structure of Turbulence in Incompressible Viscous Fluid for Very Large Reynolds Numbers, in: *Proceedings of the USSR Academy of Sciences (in Russian)*. pp. 299–303.
- Korving, H., 2004. *Probabilistic assessment of the performance of combined sewer systems*. Technical University of Delft.
- Launder, B.E., Spalding, D.B., 1974. The numerical computation of turbulent flows. *Comput. Methods Appl. Mech. Eng.* 3, 269–289. [https://doi.org/10.1016/0045-7825\(74\)90029-2](https://doi.org/10.1016/0045-7825(74)90029-2)
- Leandro, J., Chen, A.S., Schumann, A., 2014. A 2D parallel diffusive wave model for floodplain inundation with variable time step (P-DWave). *J. Hydrol.* 517, 250–259. <https://doi.org/10.1016/j.jhydrol.2014.05.020>

- Leonard, A., 1975. Energy cascade in large-eddy simulations of turbulent fluid flows. *Adv. Geophys.* 18, 237–248. [https://doi.org/10.1016/S0065-2687\(08\)60464-1](https://doi.org/10.1016/S0065-2687(08)60464-1)
- Lesieur, M., 2008. *Turbulence in Fluids*. Springer Netherlands. <https://doi.org/10.1007/978-1-4020-6435-7>
- Lopes, P., Carvalho, R.F., Leandro, J., 2017. Numerical and experimental study of the fundamental flow characteristics of a 3D gully box under drainage. *Water Sci. Technol.* 1, wst2017071. <https://doi.org/10.2166/wst.2017.071>
- Lopes, P., Leandro, J., Carvalho, R.F., Russo, B., Gómez, M., 2016. Assessment of a VOF Model Ability to Reproduce the Efficiency of a Continuous Transverse Gully with Grate. *J. Irrig. Drain. Eng.* (in production). [https://doi.org/10.1061/\(ASCE\)IR.1943-4774.0001058](https://doi.org/10.1061/(ASCE)IR.1943-4774.0001058)
- Martins, R., Leandro, J., Carvalho, R.F., 2014. Characterization of the hydraulic performance of a gully under drainage conditions. *Water Sci. Technol.* 69, 2423–30. <https://doi.org/10.2166/wst.2014.168>
- Menter, F.R., 1992. Improved two-equation k- ω turbulence models for aerodynamic flows. NASA Tech. Memo. 1–31. <https://doi.org/10.2514/6.1993-2906>
- Pfister, M., Gisonni, C., 2014. Head Losses in Junction Manholes for Free Surface Flows in Circular Conduits. *J. Hydraul. Eng.* 140, 6014015. [https://doi.org/10.1061/\(ASCE\)HY.1943-7900.0000895](https://doi.org/10.1061/(ASCE)HY.1943-7900.0000895)
- Pope, S.B., 2000. *Turbulent Flows*, 1st ed, Cambridge. Cambridge University Press, Cambridge.
- Rusche, H., 2002. *Computational Fluid Dynamics of Dispersed Two-Phase Flows at High Phase Fractions*. PhD Thesis. University of London. <https://doi.org/10.1145/1806799.1806850>
- Stovin, V.R., Bennett, P., Guymer, I., 2013. Absence of a Hydraulic Threshold in Small-Diameter Surcharged Manholes. *ASCE J. Hydraul. Eng.* 139, 984–994. [https://doi.org/10.1061/\(ASCE\)HY.1943-7900.0000758](https://doi.org/10.1061/(ASCE)HY.1943-7900.0000758)
- Tang, H., Wrobel, L.C., 2005. Modelling the interfacial flow of two immiscible liquids in mixing processes. *Int. J. Eng. Sci.* 43, 1234–1256. <https://doi.org/10.1016/j.ijengsci.2005.03.011>
- Ubbink, O., 1997. Numerical prediction of two fluid systems with sharp interfaces. *Splash*. <https://doi.org/10.1145/1774088.1774119>
- Versteeg, H.K., Malalasekera, W., 1995. *An Introduction to Computational Fluid Dynamics - The Finite Volume Method*, Fluid flow handbook. McGraw-Hill Longman Scientific and Technical, Essex, Eng.
- Weller, H.G., 2002. Derivation modelling and solution of the conditionally averaged two-phase flow equations, Technical Report TR/HGW/02, Nabla Ltd.
- Weller, H.G., Tabor, G., Jasak, H., Fureby, C., 1998. A tensorial approach to computational continuum mechanics using object-oriented techniques. *Comput. Phys.* 12, 620. <https://doi.org/10.1063/1.168744>
- Wilcox, D.C., 1988. Reassessment of the scale-determining equation for advanced turbulence models. *AIAA J.* 26, 1299–1310. <https://doi.org/10.2514/3.10041>
- Yakhot, V., Orszag, S.A., Thangam, S., Gatski, T.B., Speziale, C.G., 1992. Development of turbulence models for shear flows by a double expansion technique. *Phys. Fluids* 4, 1510–1520. <https://doi.org/10.1063/1.858424>

APPENDICES

APPENDIX 1 - Mathematical Models

Equations of Motion

Fluid is treated as a continuum and described in terms of macroscopic properties such as velocity, pressure, density, temperature and energy. The fluid flow is governed by the conservation laws of physics: conservation of mass, momentum and energy. These laws are described by equations that are the main basis of CFD and can be written in differential form (Eq. A1.1 and A1.2) as described in Batchelor (1967) and Pope (2000). Where ρ is the fluid density, u_i the three-dimensional velocity field in the Cartesian domain described by u_i (u_x, u_y, u_z), σ is the shear stress tensor, e is the total specific energy, Q is the volume energy source, e is the heat flux and g is the gravity acceleration vector.

$$\frac{\partial \rho}{\partial t} + \nabla \cdot (\rho u) = 0 \quad (\text{A7.1})$$

$$\frac{\partial \rho u}{\partial t} + \nabla \cdot (\rho u u) = \rho g + \nabla \cdot \sigma \quad (\text{A1.8})$$

Conservation of mass (Eq.A1) translates the dependency of the change in density in time with the net flow of mass across boundaries described by the convective term. In an Eulerian description, the increase of mass in the fluid element equals the net rate of flow of mass into element. In a Lagrangian description, the moving fluid particles experiences two rates of changes, due to changes in the fluid as a function of time and due to the fact that it moves to a different location in the fluid with different conditions. In most cases, we are interested in the change of a flow property for a fluid element, or fluid volume in a fixed in space.

Conservation of momentum (Eq.A2) is Newton's Second Law meaning that the rate of change of momentum equals the sum of all the forces. Surface forces such as pressure and viscous shear forces and body forces, which act on a volume, such as gravity, centrifugal, Coriolis, and electromagnetic forces are the different types of forces that can be applied on the fluid. We need to include a model for the viscous stresses which usually are expressed as functions of the local deformation rate (strain rate) tensor and we consider dynamic viscosity for the linear deformations and a second viscosity for the volumetric deformations, resulting the well-known Navier-Stokes equations.

Sometimes simplification is made in the analysis of different fluid flow problems selecting the appropriate coordinate directions so that appreciable variation of the hydrodynamic parameters take place in only two directions or even in only one direction. In fact, the flow is never one or two-dimensional (1D/2D). However we can consider it 1D or 2D if non uniformity along some other direction(s) is much less than the main flow direction.

3D Models - CFD

In 3D Models, the hydrodynamic parameters are functions of three orthogonal space coordinates and time and numerical models deal with Eqs. A1 and A2. Focusing on complete numerical solutions of the Navier-Stokes Equations (known as Direct Numerical Simulation, DNS), it is not possible to completely solve all the scales involved in turbulence dynamics (known as Kolmorov's criterion (Kolmogorov, 1941)). Filtering or ensemble average are employed to obtain Large Eddy Simulations (LES) or Reynolds-averaged Navier-Stokes equations (RANS) for practical applications of fluid flow. LES models large scales directly and represents small

scales whereas RANS approach models the motion of mean flows (Carvalho et al., 2008) and representing fluctuation by means of Reynolds stresses which need additional equations to close the system.

In LES, equations yield to Large-scale models based on the properties of the turbulent field representation by filters of different scales. Each filter is associated with a scale that separates small vortices from large scales. Later, small scales are represented at large scales through subscale models (Sub-Grid Scale, SGS). In this way, LES fit between the direct approach and the approximation presenting the advantage of being less dependent on empirical parameters and preserving the turbulence properties better. This allows modellers to obtain mean values of the time and to give an idea of the magnitude and standard deviation of the fluctuations associated to turbulent flow.

The theoretical difficulties of the filtering process of the LES equations derive from the SGS models through to the dynamic models that relate the turbulent tensors to different dynamic modelling procedures. Dynamic models usually require high computational effort, thus are applied to flows with high Reynolds Numbers. The classic formulation of dynamic models is given by Leonard (1975) and Germano (1992) gave the operational formulation of it (known as Germano's identity). The formulation is given as (in Lesieur 2008 and Carvalho, 2002):

The equation after the filter application takes the form:

$$\frac{\partial \bar{u}_i}{\partial t} + \bar{u}_j \frac{\partial \bar{u}_i}{\partial x_j} = g_i - \frac{1}{\rho} \frac{\partial \bar{p}}{\partial x_i} + \frac{\partial}{\partial x_j} \left\{ \frac{\mu}{\rho} \left(\frac{\partial \bar{u}_i}{\partial x_j} + \frac{\partial \bar{u}_j}{\partial x_i} \right) \right\} + T_{ij} \quad (\text{A1.3})$$

where, \bar{u}_i , \bar{u}_j and \bar{p} are the components of the filtered velocity vector and pressure, T_{ij} is the characteristic tensor of the microscale (subgrid-scale tensor) given by:

$$T_{ij} = \bar{u}_i \bar{u}_j - \overline{\bar{u}_i \bar{u}_j} - \overline{\bar{u}_i u_j'} + \overline{\bar{u}_j u_i'} - \overline{u_i' u_j'} \quad (\text{A1.4})$$

The first and second terms are known as the Leonard term, the third and fourth are the term crossed, and the latter is a term similar to the Reynolds tensor. The Leonard's term is an explicit term that can be computed in the filtered field, while the others are unknown. The SGS modelling is very complex, since it requires modelling and terms in the equations that allow the transfer of kinetic energy from the large scales to smaller ones or SGS. The mathematical treatment of this type of equation has successive developments in the last decade. From the simplest SGS models, based on the concept of turbulent viscosity, the best known is the Smagorinsky model that introduces the concept of turbulent viscosity proportional to the characteristic length of the subscale Δx , and to the characteristic velocity fluctuation $v_{\Delta x} = \Delta x |S|$, which is equivalent to approximate T_{ij} as:

$$T_{ij} = \frac{\mu_t}{\rho} \left(\frac{\partial \bar{u}_i}{\partial x_j} + \frac{\partial \bar{u}_j}{\partial x_i} \right) = -(C_s \Delta) S_{ij} \left(\frac{\partial \bar{u}_i}{\partial x_j} + \frac{\partial \bar{u}_j}{\partial x_i} \right) \quad (\text{A1.5})$$

where, μ_t is the turbulent viscosity coefficient, C_s is the Smagorinski constant ($C_s = 0.17$ to 0.23), Δ is the filter and S_{ij} is the strain tensor, respectively equal to:

$$\Delta = (\Delta x \Delta y \Delta z)^{1/3} \quad (\text{A1.6})$$

$$S_{ij} = \left(\frac{1}{2} \left(\frac{\partial \bar{u}_i}{\partial x_j} + \frac{\partial \bar{u}_j}{\partial x_i} \right) \right)^{1/2} \quad (\text{A1.7})$$

This approach leads to good results if the non-resolvable scales are in the viscous range. When using a minimum scale larger than scales in the viscous range, these models are referred to as Coherent Structure Capturing Models (CSCM).

The turbulence models based on the Reynolds equations allow statistical analysis of the equations of motion

and result from the consideration of Reynolds average $u_i = \bar{u}_i + u_i'$ and $\bar{u}_i \bar{\varphi} = \bar{u}_i \bar{\varphi} + \overline{u_i' \varphi'}$. From the Navier-Stokes equations applied to a viscous fluid and considering the Reynolds decomposition, the following Reynolds equations are obtained for incompressible or quasi incompressible fluids:

$$\frac{\partial \rho}{\partial t} + \frac{\partial(\rho \bar{u}_i)}{\partial x_i} = 0 \quad (\text{A1.8})$$

$$\frac{\partial \bar{u}_i}{\partial t} + \bar{u}_j \frac{\partial \bar{u}_i}{\partial x_j} = g_i - \frac{1}{\rho} \frac{\partial \bar{p}}{\partial x_i} + \frac{\partial}{\partial x_j} \left(\frac{\mu_t}{\rho} \frac{\partial \bar{u}_i}{\partial x_j} + T_{ij} \right) \quad (\text{A1.9})$$

The additional terms in the Navier-Stokes equations, $T_{ij} = \overline{u_i' u_j'}$ represent the Reynolds stresses ($\overline{\rho u_i' u_j'}$) which constitute additional unknowns. With the introduction of the Reynolds averages, a system is obtained with greater number of unknowns than equations (4 equations and 10 unknowns $p, u, v, w, u', v', w', u'v', u'w', v'w'$). The turbulence models, based on the Reynolds equations, consist of the introduction of relations that translate the behaviour of the turbulence in order to obtain a system of equations and unknowns, which can then be solved numerically (closing relations). The models can directly calculate the turbulent tensors through differential equations and are called models of turbulent stresses (Reynolds tensors), Reynolds Stress Models (RSM). These models include transport equations for all Reynolds tensors and require the simultaneous calculation of a large number of equations. Algebraic Stress Models (ASM) directly calculate the Reynolds tensors through algebraic equations.

The turbulence models based on the Reynolds equations do not describe in detail the turbulent fluctuations, considering that average quantities and the system of equations require the introduction of parameters and/or empirical coefficients for their resolution. In these models, part of the 'irregularity' of the flow is translated in the mean definition. Attention should be focused on the mean flow and the effects of turbulence on mean flow properties. When Reynolds stresses are not taken into account either by Reynolds Stress Models or additional equations, normally for kinetic energy, dissipation energy, models usually use dummy turbulence.

1D, 2D and quasi-3D Equations

A fluid flow can be considered one-dimensional whenever the flow parameters could be expressed as functions of time and one space coordinate. A fluid flow can also be considered two-dimensional if all the flow parameters are functions of time and two space coordinates. Usually we refer this as usual 2D model where the mass and momentum equations (Eq. A1.11, A1.2 and Eq. A1.8 and A1.90) are obtained by integration in depth, achieving the well-known 2D Shallow Water equation (SWE) (Eq. A1.10, A1.11 and A1.12). Averaging variables throughout its section, the 1D Shallow Water equation can be achieved.

$$\frac{\partial h}{\partial t} + \frac{\partial(hu)}{\partial x} + \frac{\partial(hv)}{\partial y} = 0 \quad (\text{A1.10})$$

$$\frac{\partial(hu)}{\partial t} + \frac{\partial(hu^2)}{\partial x} + \frac{\partial h(uv)}{\partial y} + gh \frac{\partial h}{\partial x} = -gh \frac{\partial z_b}{\partial x} - \tau_{bx} \quad (\text{A1.11})$$

$$\frac{\partial(hv)}{\partial t} + \frac{\partial h(uv)}{\partial x} + \frac{\partial(hv^2)}{\partial y} + gh \frac{\partial h}{\partial y} = -gh \frac{\partial z_b}{\partial y} - \tau_{by} \quad (\text{A1.12})$$

The majority of Urban Inundation models use the simplified forms of SWE, the Saint-Venant Equations (SVE) 1D up to SWE 2D, e.g. MIKE21, FLO- 2D, SOBEK, ISIS and TELEMAC-2D. Simpler models like Urban Inundation Model (UIM)/SIPSON (Djordjević et al., 2005) and SIPSON/Parallel Diffusive Wave Model (P-DWave) (Leandro et al., 2014) neglect the local and convective acceleration with wave diffusion and translation modelled. Propagation in these models is said to be infinite since all the acceleration terms are neglected.

SWE could be presented for steady or unsteady flows usually using as dependent variables discharge or average velocity and cross section or water depth. Below are represented usual forms of 1D SWE in function of Cross-Section and discharge.

$$\frac{\partial A}{\partial t} + \frac{\partial Q}{\partial x} = 0 \quad (\text{A1.13})$$

$$\frac{\partial Q}{\partial t} + \frac{\partial(\frac{Q^2}{A} + gI_1)}{\partial x} + gA \frac{\partial H}{\partial x} + gAS_f = 0 \quad (\text{A1.14})$$

In Eq. A1.13, the first member contains the term corresponding to the local acceleration and the term corresponding to the change of the momentum through the cross-section; the second, in turn, is composed of the convective term and the contribution of the hydrostatic pressure term; the latest identify the source terms of the momentum, namely the external forces acting on the fluid: gravitational force, resistance to flow; A is the surface area, Q is the flow discharge, H is the hydraulic head, S_f is the slope and also the energy loss along the flow (bed friction). The SWE equations are well accepted to mathematically express the physical phenomenon of a flow with the following assumptions:

- In the interface between air and water the pressure is assumed to be zero;
- The vertical component of the acceleration is neglected and the vertical pressure distribution is hydrostatic;
- Horizontal directions (x,y) acceleration and therefore velocities are independent from the vertical coordinate (z);
- The fluid is incompressible and homogeneous;
- Coriolis stresses, viscous terms and surface stress are neglected.

Valuable results may often be obtained from an one dimensional analysis in pipes or river stretches when variations of pressure and velocity occur along the length of the pipe or river stretch and the flow can be studied in terms of average velocity or discharge.

In systems composed for several pipes or stretches intersecting in nodes, a node continuity equation is added:

$$\frac{\partial h}{\partial t} = \frac{\sum q}{A_{store} + \sum A_s} \quad (\text{A1.15})$$

where, A_{store} is the surface area of the node, A_s is the contribution from the water surface area in the pipes until half the length of the conduit, and q is the contribution of inflow and outflow into the node.

When vertical variation over the water depth is significant some parametric typical vertical distribution could be taking into account in 2D models, achieving quasi-3D Models.

A 2D model considering two-dimensional x and z and no variation on transversal, y direction, should be used if all the flow parameters are functions of time and x and z space coordinates. It is a special case of 3D models where longitudinal and vertical directions are more important than the transversal direction, i.e. it is assumed to be applied to the entire transversal section as in prismatic channels with constant width or classic hydraulic jumps. In this last example in spite of the flow being highly 3D, one must be interested in characteristics along the longitudinal and vertical direction.

APPENDIX 2 - OpenFOAM®

Overview of OpenFOAM®

OpenFOAM® has a well-developed library to solve partial differential equations (PDEs), and ordinary differential equations (ODEs). The code is released as free and open source software under the GNU General Public License. It can be used on massively parallel computers. There is requirement to pay for separate licenses. It is under active development, its capabilities mirror those of commercial CFD applications. It counts with a wide-spread community around the world (industry, academia and research labs).

One distinguishing feature of OpenFOAM® is its syntax for tensor operations and partial differential equations that closely resembles the equations being solved. For example, the following equation is represented by the code below.

$$\frac{\partial \rho U}{\partial t} + \nabla \cdot \phi U - \nabla \cdot \mu \nabla U = -\nabla p \quad (\text{A2.1})$$

```
solve
(
  fvm::ddt(rho,U)
+ fvm::div(phi,U)
- fvm::laplacian(mu,U)
==
- fvc::grad(p)
);
```

This syntax, achieved through the use of object oriented programming and operator overloading, enables users to create custom solvers with relative ease. However, code customization becomes more challenging with increasing use of the OpenFOAM® library, owing to a lack of documentation, and heavy use of template metaprogramming.

Users can create custom objects, such as boundary conditions or turbulence models that will work with existing solvers without having to modify or recompile the existing source code. OpenFOAM® accomplishes this by combining virtual constructors with the use of simplified base classes as interfaces. As a result, this gives OpenFOAM® good extensibility qualities.

The software has extensive multi-physics capabilities:

- Computational fluid dynamics.
- Heat transfer and conjugate heat transfer.
- Combustion and chemical reactions.
- Multiphase flows and mass transfer.
- Stress analysis and fluid-structure interaction.
- Particle methods (DEM, DSMC, MD) and Lagrangian particles tracking.
- Dynamic mesh handling, 6 DOF solvers, and adaptive mesh refinement.
- Computational aero-acoustics, computational electromagnetics, computational solid mechanics, etc.

OpenFOAM® design encourages code and libraries re-use. As solvers can be tailored by a user for a specific need, OpenFOAM® is ideal for research and development.

Considerations of working with OpenFOAM®

One of the strengths of OpenFOAM® is that new solvers and utilities can be created by its users with some pre-requisite knowledge of the underlying method, physics and programming techniques involved. OpenFOAM is supplied with pre- and post-processing environments. The interface to the pre- and post-processing are themselves OpenFOAM® utilities, thereby ensuring consistent data handling across all environments. The overall structure of OpenFOAM® is shown in Figure A2-1.

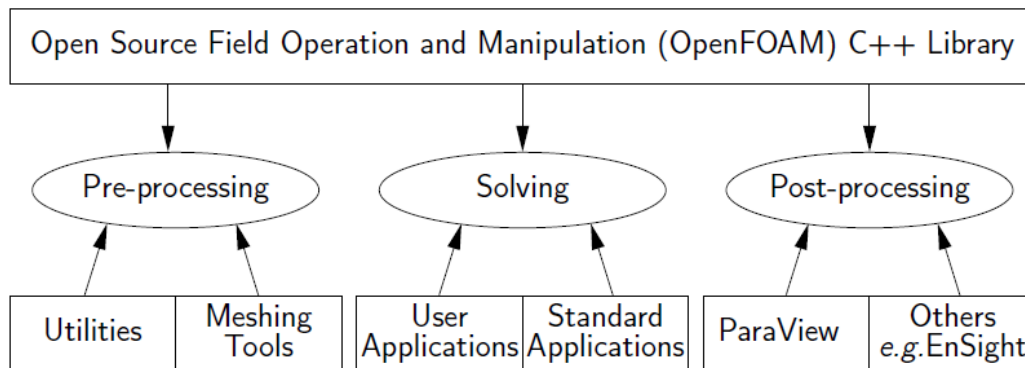


Figure A2-1: OpenFOAM® structure

OpenFOAM® operates with Finite Volume Method (FVM) based solvers. It has uses collocated polyhedral unstructured meshes. It can achieve second order accuracy in space and time. Many discretization schemes are available including high order methods. For fluid modelling, pressure-velocity coupling is done via segregated methods (SIMPLE and PISO). However, coupled solvers are also under active development.

To run an OpenFOAM® simulation, the case directory must consist of the following folder shown in Figure A2-2. Each folder contains specific information to run the simulation.

- system: contains run-time control and solver numerics.
- constant: contains physical properties and turbulence modelling properties.
- constant/polyMesh: contains the polyhedral mesh information.
- 0: contains boundary conditions and initial conditions.
- time_directories: contains the solution and derived fields

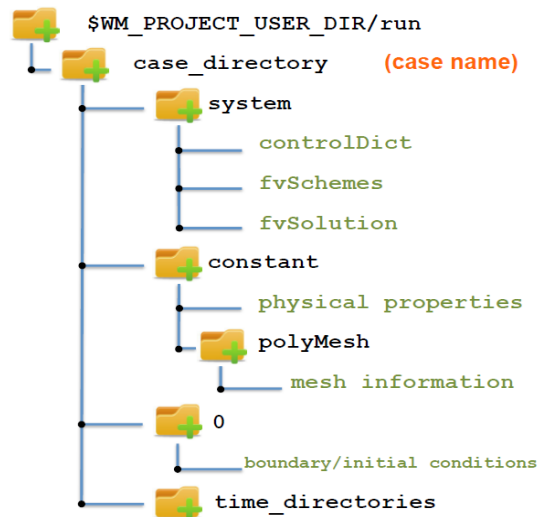


Figure A2-2: Overview of a case directory in OpenFOAM®

OpenFOAM® Mesh Generation

Mesh generation is a key part of CFD modelling. It is an integral part of the numerical solution and needs to satisfy some criteria in order to obtain a good quality of numerical solution and to ensure a valid, and hence accurate, hydrodynamic solution. During any run, OpenFOAM® checks that the mesh satisfies a fairly stringent set of validity constraints and will cease running if the constraints are not satisfied.

By default OpenFOAM® defines a mesh of arbitrary polyhedral cells in 3-D, bounded by arbitrary polygonal faces, i.e. the cells can have an unlimited number of faces where, for each face, there is no limit on the number of edges, nor any restriction on its alignment. A mesh with this general structure is known in OpenFOAM® as a polyMesh. This type of mesh offers great freedom in mesh generation and manipulation in particular when the geometry of the domain is complex or changes over time.

OpenFOAM also comes with many mesh manipulation and conversion utilities. Meshes generated using many of the major mesh generators can be converted to the OpenFOAM® format.

Basics of Mesh Generation

The effect of mesh quality is highly dependent on the flow field simulated. In regions of complex flows, with strong flow gradients, poor mesh quality (i.e. highly skewed cells), can be very damaging. However, in areas of low speed flows, the effect of such poor mesh elements is low. It is desirable to generate a high-quality mesh over the whole flow domain as prior knowledge of such areas of flow is not always possible.

Before describing the OpenFOAM® mesh format, we will first set out the validity constraints used in OpenFOAM®. The conditions that a mesh must satisfy are:

Points: A point is a location in 3-D space, defined by a vector in units of metres (m). The points are compiled into a list and each point is referred to by a label, which represents its position in the list, starting from zero. The point list cannot contain two different points at an exactly identical position nor any point that is not part of at least one face.

Faces: A face is an ordered list of points, where a point is referred to by its label. The ordering of point labels in a face is such that each two neighbouring points are connected by an edge, i.e. following points as one travels around the circumference of the face. Faces are compiled into a list and each face is referred to by its label, representing its position in the list. The direction of the face normal vector is defined by the right-hand

rule, i.e. looking towards a face, if the numbering of the points follows an anti-clockwise path, the normal vector points towards the user.

There are two types of face, Internal faces and Boundary faces. Internal faces connect two cells. A Boundary faces belongs to one cell since they coincide with the boundary of the domain. A boundary face is therefore addressed by one cell only and a boundary patch. Faces can be warped, i.e. not all points of the face need to be coplanar.

Cells: A cell is a list of faces in arbitrary order. Cells must have the following three properties:

Contiguous: The cells must completely cover the computational domain and must not overlap one another.

Convex: Every cell must be convex and its cell centre inside the cell.

Closed: Every cell must be closed, both geometrically and topologically where:

- geometrical closeness requires that when all face area vectors are oriented to point outwards of the cell, their sum should equal the zero vector to machine accuracy;
- topological closeness requires that all the edges in a cell are used by exactly two faces of the cell in question.

There are many mesh generating tools in OpenFOAM®. Some of them are described below.

BlockMesh

BlockMesh is an OpenFOAM® native option to create a computational mesh. It is the most basic mesh generators in OpenFOAM®. It relies on a single dictionary file named blockMeshDict, placed inside the folder system. The file contains information to create at least one hexahedral block. blockMesh reads this dictionary, generates the mesh and writes out the mesh data to points and faces, cells and boundary files in the constant/polyMesh folder.

The principle behind blockMesh is to decompose the domain geometry into a set of 1 or more three dimensional, hexahedral blocks. Edges of the blocks can be straight lines, arcs or splines. The mesh is specified as a number of cells in each direction of the block, sufficient information for blockMesh to generate the mesh data.

Salomé

SALOME is an open-source software that provides a generic platform for both Pre and Post Processing for numerical simulations. It is based on an open and flexible architecture made of reusable components. It can be used as a standalone application for generation of a CAD model, its preparation for numerical calculations and post-processing of the calculation results.

SALOME has several in built options to create and modify simple to complex CAD models. It supports interoperability between CAD modelling and computation software (CAD-CAE link) and makes it easier for integration of new components into heterogeneous systems for numerical computation. Salome also provides access to many functionalities via an integrated Python console.

CfMesh

cfMesh is a library for polyhedral mesh generation. The library consists of many meshing algorithms which can be reused to generate meshing workflows. It can generate 2D and 3D Cartesian meshes, 3D polyhedral, and 3D tetrahedral meshes. Meshing is a dynamic process in terms of memory allocation, and this adds extra complexity to the problem. The data containers available in cfMesh are implemented to reduce memory usage and improve performance. SMP and MPI parallelisation for performance and the ability to generate large meshes (Juretić, 2015).

Available mesh types are:

- 3D Cartesian
- Polyhedral
- Tetrahedral
- 2D Cartesian

In cfMesh, a geometry is created as a Stereo Lithography file (STL) and used as the outline of the mesh to be prepared. The meshing technology that a user needs to apply has a simple syntax, focussing on minimising user input. Most tasks are automatic. Meshing algorithms are based on an inside-out approach, which does not require watertight input geometry.

SnappyHexMesh

snappyHexMesh is used to create high quality hexahedra (hex) and split-hexahedra based meshes on arbitrary geometry. It uses *blockMesh* methodology to create different numbers of blocks in a Cartesian 3D space with different cell sizes. Later, STL geometry is used to extract the computational domain mesh region out of the pre-constructed blocks. It has some additional flexible features to refine the meshes at a different level. The surface handling is robust with a pre-specified final mesh quality. It can be run in parallel processing with a load balancing step at every iteration.

The meshing instruction has to be given through *snappyHexMeshDict* file, stored in the system folder. Some additional features can be applied to improve the mesh quality, such as:

- *castellatedMesh*: to switch on creation of the castellated mesh.
- *snap*: to switch on surface snapping stage.
- *addLayers*: to switch on surface layer insertion.
- *mergeTolerance*: merge tolerance as a fraction of bounding box of initial mesh.
- *geometry*: sub-dictionary of all surface geometry used.
- *castellatedMeshControls*: sub-dictionary of controls for castellated mesh.
- *snapControls*: sub-dictionary of controls for surface snapping.
- *addLayersControls*: sub-dictionary of controls for layer addition.
- *meshQualityControls*: sub-dictionary of controls for mesh quality.

Pre-processing: Initial and Boundary Conditions

Initial and boundary conditions should be defined by creating files for each variable in the “0” folder and informing by means of the *setfieldsDict* dictionary, in system folder, which may specify default values as well as regions with different values to define special initial conditions. The boundary is broken into **patches** (regions), where each patch in the list has its name given by the user, which should be something that conveniently identifies the patch. The name is used as an identifier for setting boundary conditions in the field data files. The patch information is then contained in sub-dictionary with:

type: the patch type, either a generic patch on which some boundary conditions are applied or a particular geometric condition;

faces: a list of block faces that make up the patch and whose name is the choice of the user, although it is

recommend to use a name that conveniently identifies the patch,

NOTE: There are a lot of possibilities to define boundary conditions in OpenFOAM® choosing between basic, primitive and derived types. The basic type includes patch, symmetryPlane, Empty, wedge, cyclic, wall, and processor. Primitive type includes fixedValue, fixedGradient, zeroGradient, Calculated, Mixed and directionMixed. For Derived type, each of the presented types are available.

The "constant" folder includes property files related to the physical, thermodynamic or fluid turbulence properties: usually, the "g", "transportProperties" and "turbulenceProperties" files are present. Finally, in the "system" directory there are "controlDict", which contains the simulation time information (initial and final), calculation step, data writing interval or Courant maximum number, the "fvSolution" that holds the information on linear system solution methods, "fvSchemes" that inculcates to the simulation the discretization / interpolation methodologies of the terms of the equations and the dictionary "setFieldsDict" where the global initial conditions of the model are programmed.

SOLVER

OpenFOAM® comes with several ready-to-use or user defined solvers. The available solvers can be categorised as follows:

- Basic solvers: Laplace, potential flow, passive scalar transport.
- Incompressible and compressible flows: segregated pressure-based algorithms (SIMPLE and PISO).
- Heat transfer modelling capabilities: buoyancy-driven flows, conjugate heat transfer.
- Multiphase flows: Euler-Euler, VOF for free surfaces, multiple phases, cavitation, and phase change.
- Combustion and fire dynamic solvers.
- Stress analysis, electromagnetics, acoustics, MHD, fluid structure interaction, etc.

Despite having several solvers, one can implement a solver of their own in OpenFOAM®. It is designed to be a flexible and programmable environment for numerical simulations by using a high level programming language that is a direct representation of the equations being solved. New solvers can also be easily implemented using OpenFOAM® by mimicking equations.

InterFoam solver

Three dimensional flow in urban drainage is free-surface flow and can be modelled with air and possibly sediment concentration within. The interFoam solver in OpenFOAM® toolbox is a solver that includes VOF method presented by Hirt and Nichols (1981). The mathematical formulation of interFoam is described here which closely the works of Jasak (1996), Ubbink (1997) and Rusche (2002) in developing the solver.

Continuity and Momentum Equations

Fluid flow is mainly governed by conservation of mass, momentum and energy equations. These equations are the main basis of interFoam solver. The solver interFoam assumes the fluids as Newtonian, isothermal ($q=0$) and incompressible (ρ is constant). As mentioned in Jasak (1996), the three equations (A1.1, A1.2 and A1.3) can be simplified in the following form:

$$\nabla \cdot u = 0 \quad (\text{A2.220})$$

$$\frac{\partial u}{\partial t} + \nabla \cdot (uu) = g - \nabla p + \nabla \cdot (\nu \nabla u) \quad (\text{A2.391})$$

where, ν is the kinematic viscosity and p the kinematic pressure. Multiplying the momentum equation by the density of the fluid and considering surface tension influence, the final form of the momentum equations for a single field of fluid becomes:

$$\frac{\partial \rho u}{\partial t} + \nabla \cdot (\rho u u) = -\nabla P + \nabla \cdot \tau + \rho g + F \quad (\text{A2.4})$$

where, P is the pressure ($P = p \times \rho$), τ is the viscosity stress tensor and F represents the source of the momentum in regard to the surface tension (Rusche, 2002):

$$F = \int_{S(t)} \sigma \kappa n \delta(x - \hat{x}) dS \quad (\text{A2.5})$$

In the equation above, σ represents the surface tension coefficient, κ denotes the curvature and n is the normal vector of the interface. The viscous stress term can be rewritten to obtain more efficiency in the following form:

$$\nabla \cdot \tau = \nabla \cdot (\mu [\nabla u + (\nabla u)^T]) = \nabla \cdot (\mu \nabla u) + (\nabla u) \cdot \nabla \mu \quad (\text{A2.6})$$

The modified pressure p^* ($p = \rho g h$ in OpenFOAM® code) is adopted in interFoam removing the hydrostatic pressure ($\rho g \cdot x$) from the pressure P . This formulation gives more advantages in applying boundary conditions (Rusche, 2002). The gradient of the modified pressure is defined as:

$$\nabla p^* = \nabla P - \nabla(\rho g \cdot x) = \nabla P - \rho g - g \cdot x \nabla \rho \quad (\text{A2.7})$$

The volume fraction is an indicator function (alpha in OpenFOAM® code) to define the portion of the cell is occupied by the fluid equation.

$$\alpha(x, y, z, t) = \begin{cases} 1 & \text{for a place } (x, y, z, t) \text{ occupied by fluid 1} \\ 0 < \alpha < 1 & \text{for a place } (x, y, z, t) \text{ occupied by interface} \\ 0 & \text{for a place } (x, y, z, t) \text{ occupied by fluid 2} \end{cases} \quad (\text{A2.8})$$

The transport of α in time, is expressed by an advection equation:

$$\frac{\partial \alpha}{\partial t} + \nabla \cdot (\alpha u) = 0 \quad (\text{A2.9})$$

The fluid properties (ρ and μ) are calculated according to the volume fraction of each fluid:

$$\rho = \alpha \rho_1 + (1 - \alpha) \rho_2 \quad (\text{A2.10})$$

$$\mu = \alpha \mu_1 + (1 - \alpha) \mu_2 \quad (\text{A2.11})$$

In case of an incompressible fluid, conservation of volume is equivalent to conservation of mass and thus with conservation of mass, conservation of α is necessary, particularly in the case of high density fluids, where small errors on the volume fraction generate significant errors on the physical properties and, to respond to this issue, many researchers have been presenting alternative techniques to overcome this problem (Ubbink, 1997). The best alternative was formulated by Weller (2002), introducing an extra term in the phase fraction function, which is known as artificial compression term.

$$\frac{\partial \alpha}{\partial t} + \nabla \cdot (\alpha \bar{u}) + \underbrace{\nabla \cdot [\mathbf{u}_r \alpha (1 - \alpha)]}_{\text{artificial compression term}} = 0 \quad (\text{A2.11})$$

where, \mathbf{u}_r is the relative velocity vector between the two fluids; also called as compression velocity (Berberovic et al., 2009) such as:

$$u_r = u_1 - u_2 \quad (\text{A2.12})$$

Mean velocity is calculated by a weighted average of the velocity between the two fluids:

$$\underline{u} = \alpha u_1 + (1 - \alpha) u_2 \quad (\text{A2.13})$$

Surface Tension Force

The surface tension force acts on the interface between the two phases. But in the model, interface is not tracked explicitly and the exact location is unknown (Rusche, 2002). Therefore, the source term (F) in the momentum equation related to the surface tension force, cannot be calculated. The Continuum Surface Force (CSF) model developed by Brackbill et al. (1992) interprets the F term in terms of volume force function and solves this issue. In this CSF model, the surface curvature (κ) is formulated from local gradients in the surface normal (n) at the interface, which is a function of the phase fraction ($n=\nabla\alpha$) (Tang and Wrobel, 2005):

$$\kappa = \nabla \cdot \hat{n} = \nabla \cdot \frac{n}{|n|} = \nabla \cdot \left(\frac{\nabla\alpha}{|\nabla\alpha|} \right) \quad (\text{A2.14})$$

The volumetric surface tension force (F) is written in terms of the surface tension, and subsequently, to the jump pressure across the interface.

$$F = \sigma\kappa \frac{\rho}{0.5(\rho_1 + \rho_2)} \nabla\alpha \cong \sigma\kappa\nabla\alpha \quad (\text{A2.15})$$

Taking into account the volumetric form of surface tension, the viscous stress term and the modified pressure, the final form of the momentum equation is:

$$\frac{\partial\rho u}{\partial t} + \nabla \cdot (\rho uu) - \nabla \cdot (\mu\nabla u) = -\nabla p^* + (\nabla u) \cdot \nabla\mu - g \cdot x\nabla\rho + \sigma\kappa\nabla\alpha \quad (\text{A2.16})$$

The final sets of equations for the mathematical model formulations are continuity equation, the modified indicator function and the momentum equation. These equations are solved together with the constitutive relations for density and dynamic viscosity.

Turbulence Modelling

RANS (Reynolds Average Navier-Stokes) turbulence modelling approach is the most commonly used. There are several RANS models. Any of them can be applied within interFoam. However, use of k- ϵ model is the most common in engineering applications.

The standard k- ϵ model (Launder and Spalding, 1974) is based on two equations; one for k (turbulent kinetic energy) and another for ϵ (viscous dissipation). To integrate the wall turbulence effect in the model at high Reynolds number flow, the standard k- ϵ needs to integrate wall turbulence functions (Versteeg and Malalasekera, 1995). An improvement in standard k- ϵ model, made by Yakhot et al. (1992) was to remove the small scales of motion from the governing equations and represent their effects in the large scales. This process is named as Re-Normalization Group (RNG). The k- ω model suggested by Wilcox (1988) introduced a new term named turbulence frequency ($\omega=\kappa/\epsilon$) as second variable and used as alternative to the k- ϵ model. It has been observed that k- ω model gave good prediction at the near wall flow turbulence and k- ϵ showed good prediction at the fully turbulent zone. Another model proposed by Menter (1992) suggested a model between the k- ϵ and k- ω which implemented k- ω model near the walls, k- ϵ model at turbulent region of the flow. This model is known as SST k- ω model.

Running InterFoam solver

Typing the name of the solver makes OpenFOAM® run the solver, accordingly the parameters used are defined in the files placed on the system folder. For saving a history of the simulation it should be indicated the solver together with the name of the file in which to record this history. If parallel processing is wanted, the dictionary "decomposeParDict" in the must be included in "system". The dictionary must take into account the number of subdomains and the division method. For the case of 4 subdomains to be used, divided in a simple way into 2 pieces in the x direction, 2 pieces in the y direction and 1 pieces in the z

direction is defined as simpleCoeff (2 2 1). A batch file could be define to prepare all files and indicate the instructions sequentially to run.

Post-Processing

OpenFOAM® post processing is performed with ParaView, an open source cross-platform data visualisation and analysis software, developed by Sandia National Laboratory, Kitware Inc. and Los Alamos National Laboratory and using the VTK preview library. This viewer can be installed when installing OpenFOAM® through existing repositories made available by OpenCFD. It should be noted that ParaView is available for different operating systems such as Linux, Windows or Mac OS X in both 32-bit and 64-bit versions.